Short Article

Developmental Cell

Tumor-Derived Ligands Trigger Tumor Growth and Host Wasting via Differential MEK Activation

Graphical Abstract

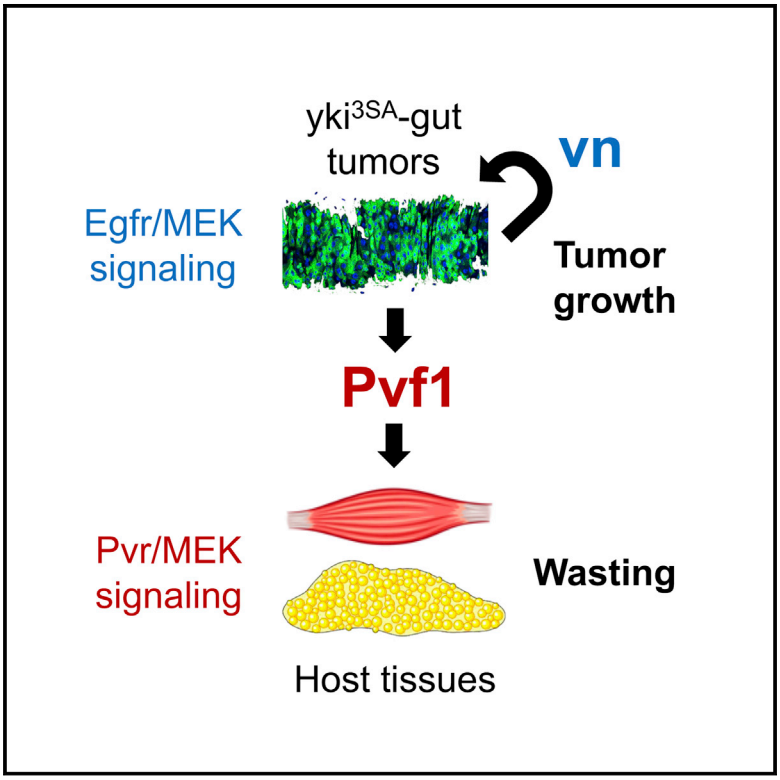

Authors

Wei Song, Serkan Kir, Shangyu Hong, ..., Alexander S. Banks, Bruce Spiegelman, Norbert Perrimon

Correspondence

songw@whu.edu.cn (W.S.), perrimon@receptor.med.harvard.edu (N.P.)

In Brief

Mechanisms of tumor-induced host wasting are largely unknown. Song et al. provide evidence that tumor-derived ligands trigger tumor growth and host wasting via differential MEK activation. They demonstrate that yki^{3SA}-gut tumors produce vn and Pvf1 ligands to trigger MEK-associated tumor growth and host wasting, respectively.

Highlights

- yki^{3SA} tumors activate systemic MEK signaling to cause tumor growth and host wasting
- Pharmaceutical MEK inhibition in host tissues alone alleviates wasting
- yki^{3SA} tumors produce vn to autonomously promote MEK signaling and tumor growth
- yki^{3SA} tumors produce Pvf1 to non-autonomously trigger host MEK signaling and wasting

Song et al., 2019, Developmental Cell *48*, 1–10
January 28, 2019
https://doi.org/10.1016/j.devcel.2018.12.003

CellPress

Please cite this article in press as: Song et al., Tumor-Derived Ligands Trigger Tumor Growth and Host Wasting via Differential MEK Activation, Developmental Cell (2018), https://doi.org/10.1016/j.devcel.2018.12.003

Developmental Cell
Short Article

Tumor-Derived Ligands Trigger Tumor Growth and Host Wasting via Differential MEK Activation

Wei Song,[1,2,8,*] Serkan Kir,[3,4] Shangyu Hong,[5] Yanhui Hu,[2] Xiaohui Wang,[2,6] Richard Binari,[2] Hong-Wen Tang,[2] Verena Chung,[2] Alexander S. Banks,[5] Bruce Spiegelman,[3] and Norbert Perrimon[2,7,*]
[1]Medical Research Institute, School of Medicine, Wuhan University, Wuhan 430071, China
[2]Department of Genetics, Harvard Medical School, Boston, MA 02115, USA
[3]Department of Cancer Biology, Dana-Farber Cancer Institute, Harvard Medical School, Boston, MA 02215, USA
[4]Department of Molecular Biology and Genetics, Koç University, Istanbul 34450, Turkey
[5]Division of Endocrinology, Diabetes and Hypertension, Brigham and Women's Hospital, Boston, MA 02115, USA
[6]Department of General Surgery, Xuanwu Hospital, Capital Medical University, Beijing 100053, China
[7]Howard Hughes Medical Institute, Boston, MA 02115, USA
[8]Lead Contact
*Correspondence: songw@whu.edu.cn (W.S.), perrimon@receptor.med.harvard.edu (N.P.)
https://doi.org/10.1016/j.devcel.2018.12.003

SUMMARY

Interactions between tumors and host tissues play essential roles in tumor-induced systemic wasting and cancer cachexia, including muscle wasting and lipid loss. However, the pathogenic molecular mechanisms of wasting are still poorly understood. Using a fly model of tumor-induced organ wasting, we observed aberrant MEK activation in both tumors and host tissues of flies bearing gut-yki^{3SA} tumors. We found that host MEK activation results in muscle wasting and lipid loss, while tumor MEK activation is required for tumor growth. Strikingly, host MEK suppression alone is sufficient to abolish the wasting phenotypes without affecting tumor growth. We further uncovered that yki^{3SA} tumors produce the vein (vn) ligand to trigger autonomous Egfr/MEK-induced tumor growth and produce the PDGF- and VEGF-related factor 1 (Pvf1) ligand to non-autonomously activate host Pvr/MEK signaling and wasting. Altogether, our results demonstrate the essential roles and molecular mechanisms of differential MEK activation in tumor-induced host wasting.

INTRODUCTION

Many patients with advanced cancer exhibit a systemic wasting syndrome, referred to as "cancer cachexia," with major features of progressive loss of muscle and adipose tissues. Cachexia is associated with poor chemotherapy response, reduced life quality, and increased mortality (Fearon et al., 2013). Unlike malnutrition conditions, cachexia can rarely be reversed by nutritional supplementation and is frequently accompanied with hyperglycemia (Chevalier and Farsijani, 2014). A number of findings in cultured cells have indicated that in addition to systemic inflammatory responses, tumors produce secreted factors (e.g., interleukins and activins) that directly target myotubes and adipocytes to cause myotube wasting and lipid loss, respectively (Miyamoto et al., 2016). Antibody neutralization of tumor-derived cachectic ligands (PTHrP) also significantly improves host wasting (Kir et al., 2014). Despite these advances, genetic animal models to comprehensively assess tumor-secreted ligands, the signaling pathways they regulate, and their effects in various tissues are far less established.

The adult *Drosophila* midgut has emerged as a model system to study tumorigenesis. Many mutations involved in human cancer have been found to result in overproliferation of fly intestinal stem cells (ISCs) and tumor formation (Patel and Edgar, 2014). The fly midgut has also been established as a conserved genetic model to study tumor-induced host wasting. We found that induction of an active oncogene *yorkie* (*yki^{3SA}*), the homolog of human Yap1, that causes gut tumor formation is associated with organ wasting phenotypes, including muscle dysfunction, lipid loss, and hyperglycemia. Mechanisms included that yki^{3SA}-gut tumors produce the IGF-antagonizing peptide ImpL2 that suppresses systemic insulin signaling and anabolism and contributes to host wasting (Kwon et al., 2015). In addition, ImpL2 regulation of host wasting has also been observed in transplanted tumors that are generated from fly imaginal discs (Figueroa-Clarevega and Bilder, 2015). Together, these findings emphasize that communication between tumor and host organs is a general phenomenon, and that *Drosophila* can be used to dissect the molecular mechanisms involved in tumor-host interaction.

The MEK/ERK cascade is a highly conserved mitogen-activated protein kinase (MAPK) pathway involved in various biological regulations in both fly and mammals (Friedman and Perrimon, 2006). MEK signaling, in addition to controlling cell proliferation, promotes muscle atrophy via modulation of ubiquitin-dependent protein degradation and enhances lipid mobilization via modulating GPCR/cAMP cascade (Hong et al., 2018; Zheng et al., 2010). These results indicate that MEK signaling is associated with loss of muscle and adipose tissues, the main features of cancer cachexia, and suggest that

MEK activation may be involved in tumor-induced host wasting. However, administration of MEK inhibitors in tumor-bearing mice and patients are associated with inconsistent results (Au et al., 2016; Prado et al., 2012; Quan-Jun et al., 2017).

In this study, we revealed aberrant MEK activation in both tumors and host tissues (muscle and fat body) of flies bearing yki^{3SA}-gut tumors. In the context of gut-tumor growth, pharmaceutical inhibition of MEK signaling in the host tissues alone is sufficient to alleviate host wasting, including muscle wasting, lipid loss, hyperglycemia, and elevated mortality, in tumor-bearing flies. Integrating RNA sequencing (RNA-seq) and RNA interference (RNAi) screening, we demonstrate that yki^{3SA}-gut tumors produce the Pvf1 ligand to activate MEK signaling and enhance catabolism in host tissues. yki^{3SA}-gut tumors also produce the vn ligand to autonomously promote MEK signaling and self-growth.

RESULTS

MEK Activation in yki^{3SA}-Tumor-Bearing Flies Contributes to Wasting of Host Tissues

To analyze the role of MEK/ERK signaling in tumor-host interaction, we first examined whether MEK signaling is activated in host tissues during tumor-induced wasting. We expressed an activated form of yorkie (yki^{3SA}, *yki$^{S111A-S168A-S250A}$* triple mutant) in adult ISCs using the temperature-sensitive GAL4 driver to trigger the development of GFP-labeled gut tumors (*esg-GAL4, tub-GAL80^{TS}, UAS-GFP/+; UAS-yki^{3SA}/+*, referred to as yki^{3SA} tumors) and host wasting (Figures 1A and S1A–S1G). Interestingly, the canonical readout of MEK signaling, pdERK (encoded by *rl*), in the muscle and fat body remained unchanged at day 2 of tumor induction (referred to as the "proliferation" state) but was significantly increased at day 4 (yki^{3SA} tumors expand to the whole midgut [referred to as the "tumorigenesis" state]), day 6 (tumor-bearing flies exhibit swollen abdomen and moderate TAG decrease and muscle dysfunction [referred to as the "ascites" state]), and day 8 (tumor-bearing flies exhibit translucent abdomen, severe TAG decrease and carbohydrate increase, and muscle dysfunction [referred as the "wasting or bloating" state]) (Figures 1A–1C and S1A–S1G). These observations indicate that MEK signaling is activated in host tissues during yki^{3SA}-tumor-induced wasting.

Further, we manipulated MEK signaling specifically in wild-type muscle or fat body. Consistent with yki^{3SA}-tumor-bearing flies (Figures S1E–S1G), specific activation of MEK signaling via expression of an activated form of *Raf* (*Raf ^{F179}*) or simply wild-type dERK in the wild-type muscle resulted in muscle-wasting phenotypes, including enhanced muscular protein degradation, impairment of myofiber integrity (gaps between myofibers and mitochondria as indicated), and climbing defects (Figures 1D–1G). MEK suppression via dERK knockdown in wild-type muscles decreased protein degradation and improved fly climbing ability (Figures 1D–1G). MEK signaling manipulation in wild-type fat bodies significantly affected lipolysis rate and lipid storage (Figures 1H–1K, and S1H), phenocopying lipid dysregulation in yki^{3SA}-tumor-bearing flies (Figures S1A and S1I). Thus, our results demonstrate that MEK activation in host tissues results in muscle wasting and lipid loss.

Autonomous MEK Activation Is Essential for yki^{3SA}-Tumor Growth

We next tested whether host MEK inhibition is sufficient to alleviate tumor-induced wasting. As systemic disruption of MEK signaling causes developmental lethality, we fed flies trametinib (Tram), an efficient MEK inhibitor (Slack et al., 2015). We initially fed flies normal food containing 10 μM or 100 μM Tram at tumor initiation (day 0). Both doses resulted in the strong MEK suppression in host tissues and diminished the bloating or wasting phenotypes of yki^{3SA}-tumor-bearing flies at day 8 (Figures 2A and 2B). However, we observed a strong reduction of yki^{3SA}-tumor growth in the midgut (Figure 2A), suggesting that MEK activation is crucial for yki^{3SA}-tumor growth. Consistently, we observed a robust increase of pdERK in yki^{3SA}-tumor gut cells (Figure 2C). Specific dERK knockdown in yki^{3SA} tumors was sufficient to terminate tumor growth (Figure 2D and S1J–S1K). However, dERK gain of function alone in ISCs only slightly increased ISCs' proliferation but failed to cause bloating/wasting (Figures S1L–S1N). Altogether, our results indicate that autonomous MEK activation in ISCs is required for yki^{3SA}-tumor growth but is not sufficient to induce host wasting.

Host MEK Inhibition Is Sufficient to Suppress yki^{3SA} Tumor-Induced Wasting

To further investigate the role of MEK signaling in host tissues in the context of yki^{3SA}-tumor growth, we fed yki^{3SA}-tumor-bearing flies Tram with a lower dosage after tumor formation from day 4 (Figures S2A and S2B). 1, 10, and 100 μM Tram significantly decreased pdERK in both muscles and fat body of yki^{3SA}-tumor-bearing flies in a dose-dependent manner (Figure S2D). 100 μM Tram still terminated, while 1 and 10 μM Tram hardly affected, yki^{3SA}-tumor growth at day 8 (Figure S2C). Strikingly, 1 and 10 μM Tram potently alleviated wasting phenotypes, including abdomen bloating, muscle degeneration, lipid loss, and hyperglycemia in the presence of yki^{3SA} tumors (Figures S2C–S2K). To validate the direct effect of Tram on host tissues, we treated isolated adult fat bodies from yki^{3SA}-tumor-bearing flies with Tram *in vitro* and confirmed that Tram robustly suppressed yki^{3SA}-tumor-induced lipolysis (Figure S1I). Similar to wasting-associated mortality of cancer patients (Fearon et al., 2013), yki^{3SA}-tumor-bearing flies also exhibited a shortened lifespan, while it was surprisingly extended by 1 and 10 μM Tram (Figures S2L–S2M). Note that feeding 1 μM Tram did not affect yki^{3SA}-tumor growth even at day 30 when most yki^{3SA}-tumor-bearing flies died (Figure S2N).

To further exclude the drug effect on yki^{3SA}-gut tumors and evaluate the impact of MEK signaling in host tissues only, we generated drug-resistant yki^{3SA} tumors by specifically overexpressing an active form of dERK (encoded by *rl^{SEM}*) (*esg-GAL4, tub-GAL80^{TS}, UAS-GFP/UAS-rl^{SEM}; UAS-yki^{3SA}/+*, referred to as "yki^{3SA}+dERK^{SEM} tumor"). Feeding 10 μM Tram simultaneously at yki^{3SA}+dERK^{SEM} tumor initiation from day 0 could no longer affect gut-tumor growth at day 8 (Figures 2E and 2F), while dramatically decreasing host MEK activation (Figure 2G). Strikingly, bloating/wasting phenotypes, including muscle defect, lipid loss, hyperglycemia, and mortality were significantly alleviated (Figures 2F–2J). Note that Tram administration in control flies (*esg-GAL4, tub-GAL80^{TS}, UAS-GFP/+*) rarely affected wasting effects (Figures S3A and S3B). We also confirmed the anti-wasting effects of another MEK inhibitor,

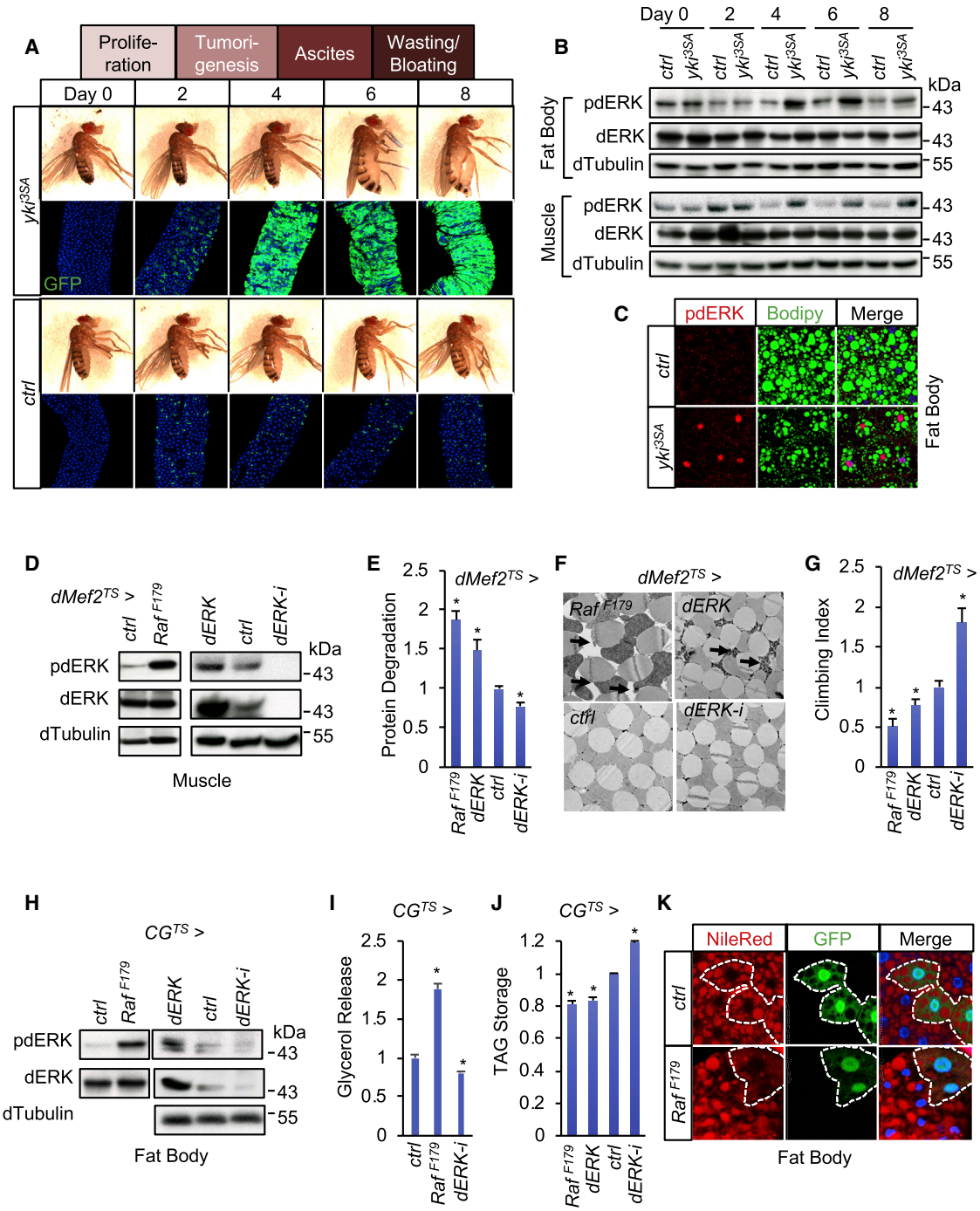

Figure 1. MEK Activation in Host Tissues of yki^{3SA}-Tumor-Bearing Flies

(A and B) Changes in the bloating appearance (A) (bright field), (gut tumors) (A) (fluorescent) (green), and pdERK in the fat body and muscles (B) of yki^{3SA}-tumor-bearing (*esg-GAL4, UAS-GFP, tub-GAL80^{TS} /+; UAS-yki^{3SA}/+*) (*yki^{3SA}*) and control (*ctrl*) (*esg-GAL4, UAS-GFP, tub-GAL80^{TS} /+*) flies.

(C) pdERK and Bodipy staining (lipid) in the fat bodies at day 6.

(D–G) Muscle pdERK (D), protein degradation rates (E) (n = 3, 30 flies/group), degenerative phenotypes (F) (arrow indicates impaired myofibril integrity), and climbing speeds (G) (centimeter/sec, normalized to control, n = 60) of *dMef2-GAL4, tub-GAL80^{TS} > UAS* flies after 8 days at 29°C.

(H–J) pdERK (H) and *in vitro* lipolysis rates in the fat body (I) (mg released glycerol/mg protein/hr, normalized to control, n = 3, 30 abdomens/group) and lipid storages (J) (mg TAG/mg protein, normalized to control, n = 3, 30 flies/group) of *CG-GAL4, tub-GAL80^{TS} > UAS* flies after 8 days at 29°C.

(K) Nile Red staining (lipid) in adult fat body clones after transgene induction for 3 days.

Data are presented as means ± SEM. *p < 0.05.

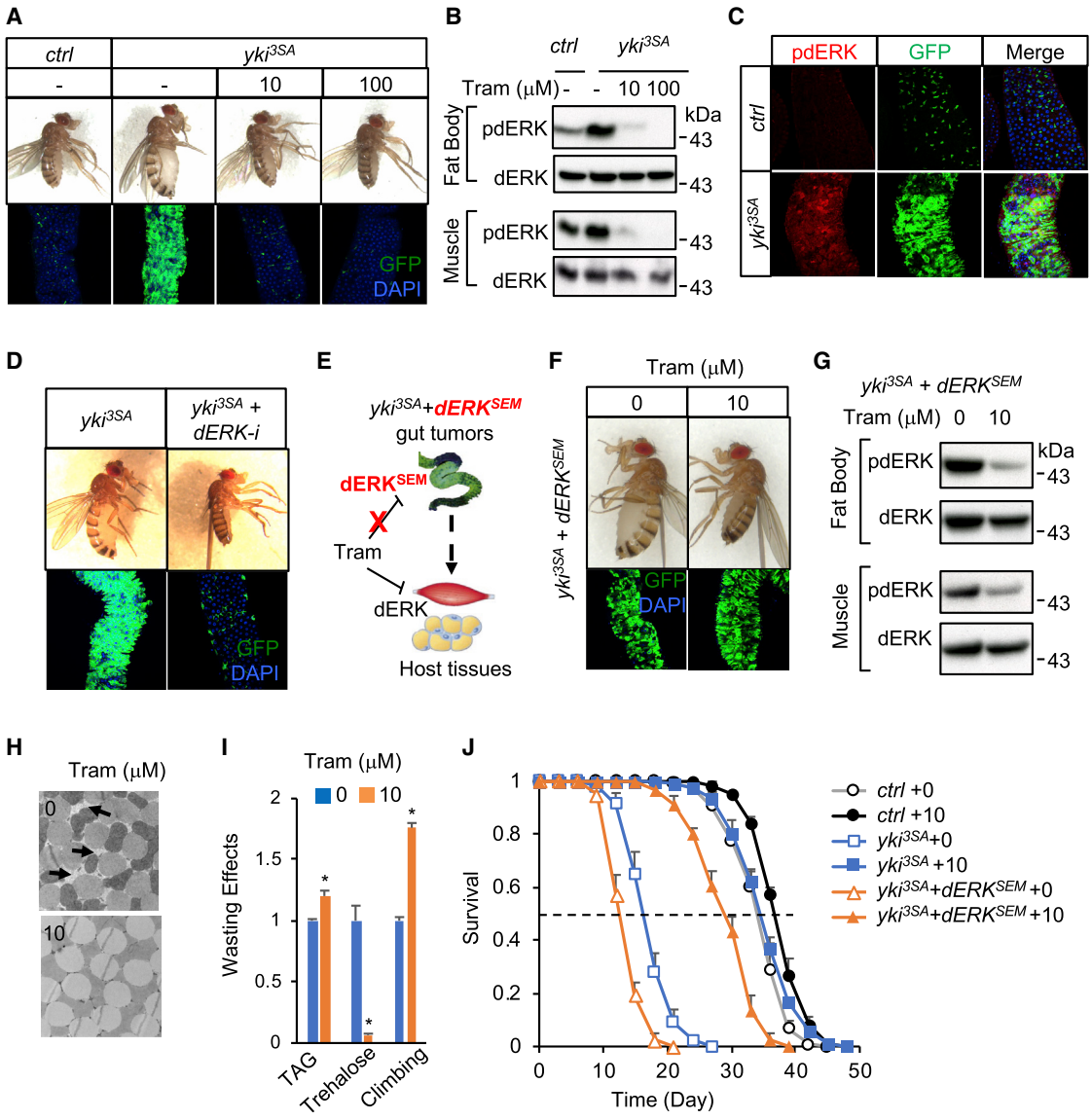

Figure 2. Pharmaceutical MEK Inhibition in Host Tissues Abolishes yki^{3SA} Tumors-Induced Wasting

(A and B) Bloating phenotypes (A) (up), gut tumors (A) (down), and pdERK in the fat body and muscles (B) were measured after Tram treatment with tumor induction simultaneously, for 8 days.

(C) pERK in yki^{3SA}-tumor midgut at day 8.

(D) Bloating (up) and gut tumors (down) of flies bearing yki^{3SA}-gut tumors with dERK-RNAi (*esg-GAL4, UAS-GFP, tub-GAL80^{TS} /+; UAS-yki^{3SA}/UAS-dERK-RNAi*).

(E) Schematic host MEK suppression by Tram in yki^{3SA}+dERK^{SEM} tumor-bearing flies (*esg-GAL4, UAS-GFP, tub-GAL80^{TS} /UAS-dERK^{SEM}; UAS-yki^{3SA}/+*).

(F–J) Wasting phenotypes of flies treated with Tram and yki^{3SA}+dERK^{SEM} tumor induction simultaneously, for 8 days. Bloating (F) (up), gut tumors (F) (down), pdERK (G), muscle degeneration (H), lipid and trehalose storage (I) (n = 3, 30 flies/group), climbing speed (I) (n = 60), and lifespan (J) (n = 120). Genotype of *ctrl* is *esg-GAL4, UAS-GFP, tub-GAL80^{TS}/+*.

Data are presented as means ± SEM. *p < 0.05.

PD0325901 (PD), in flies bearing yki^{3SA}+dERK^{SEM} tumors (Figures S3C–S3E, albeit at a higher dose). Collectively, our results demonstrate that host MEK suppression is sufficient to improve yki^{3SA}-tumor-induced wasting.

MEK Activation Contributes to LLC-Induced Wasting of Adipocytes and Myotubes

We next tested whether the similar effects of MEK activation could be observed in mammalian wasting models. Conditioned medium from mouse LLC (Lewis lung carcinoma) cancer cells strongly induces lipid loss in adipocytes and myotube atrophy (Rohm et al., 2016; Zhang et al., 2017). We found that LLC-conditioned medium activates MEK signaling in both cultured C2C12 myotubes and 3T3-L1 adipocytes after 15 min treatment (Figures S4A and S4F). Interestingly, LLC-conditioned medium robustly resulted in, while adding Tram significantly alleviated, MEK-associated induction of ubiquitination-related genes (*UbC* and *USP19*) and protein degradation, decrease of MHC

level, and atrophy phenotype in C2C12 myotubes (Liu et al., 2011; Zheng et al., 2010) (Figures S4A–S4E). Similarly, LLC-conditioned medium potently enhanced, while adding Tram significantly hampered, lipolysis rate and TAG decline in differentiated 3T3-L1 adipocytes (Figures S4F–S4I). Thus, our results demonstrate that MEK activation also causes tumor-induced wasting in mammalian myotubes and adipocytes.

Using RNA-Seq and RNAi Screening to Identify yki^{3SA}-Tumor-Derived Cachectic Ligands

We hypothesized that MEK non-autonomous regulation of host wasting is caused by secreted proteins from yki^{3SA}-gut tumors. To identify such factors, we characterized the transcriptomic changes in yki^{3SA}-tumor midguts using RNA-seq. Following statistical analysis, 2,211 genes were found to be significantly changed (fold change > 2) encompassing 1,659 up- and 552 down-regulated genes in yki^{3SA} midguts (Figure 3A; Table S1). Among the 794 genes encoding secreted proteins annotated by GLAD Gene Ontology (Hu et al., 2015), 92 were significantly up-regulated and 36 were down-regulated (Table S1). Genes encoding different trypsins were the most differentially regulated in yki^{3SA}-tumor guts (Figure S3F, up). As flies bearing yki^{3SA} tumors did not exhibit a digestion or absorption problem (Kwon et al., 2015), we speculate that yki^{3SA} tumors only change the composition of trypsin production but do not affect trypsin-associated nutrient absorption in the gut. Interestingly, the transcriptional levels of gut hormones, which are produced in enteroendocrine cells (EEs) (Reiher et al., 2011; Song et al., 2017a; Song et al., 2014), were decreased in yki^{3SA} midguts (Figure S3F, down). Immunostainings also revealed that EEs (Pros^{+} cells) were largely missing in yki^{3SA} midguts (Figure S3G). We next asked whether yki^{3SA}-gut tumors cause host wasting via loss of EEs and gut hormones, and overexpressed an active form of Notch (N^{act}) in ISCs to genetically suppress EE generation in the midgut (Takashima et al., 2011). Consistently, ISC overexpression of N^{act} potently eliminated EEs in the midgut (Figure S3G) but failed to affect bloating/wasting effects (Figure S3H). N^{act} overexpression slightly reduced survival rates of flies (Figure S3I), but the extent of decline was very marginal as compared to yki^{3SA}-tumor-bearing flies.

We next hypothesized that yki^{3SA}-gut tumors cause host wasting via increasing the production of a cachectic ligand(s) such as ImpL2. We thus performed an RNAi screening of most up-regulated ligand-encoding genes in yki^{3SA} tumors (Figure 3B). Interestingly, knockdown of 39 ligand-encoding genes (60 RNAi lines) in yki^{3SA}-gut tumors still exhibited both tumor growth and abdomen bloating. However, knockdown of 17 ligand-encoding genes (24 RNAi lines) in yki^{3SA}-gut tumors (referred to as Group "Tumor without Bloating") diminished bloating without affecting tumor growth, suggesting that these ligands regulate tumor-induced wasting. Knockdown of 8 genes (11 RNAi lines) (referred to as Group "Non-tumor") exhibited no tumor growth, suggesting that these ligands are essential for yki-induced tumorigenesis (Figure 3C; Table S2).

yki^{3SA} Tumors Produce vn to Autonomously Promote Egfr/MEK-Induced Tumor Growth

Among the established MEK-activating ligands that are induced in yki^{3SA}-tumor guts (Figures 3D and S3J), only *Pvf1* knockdown in yki^{3SA} tumors potently abolished the bloating phenotypes without perturbing yki^{3SA}-tumor growth, while only *vn* knockdown terminated yki^{3SA}-tumor growth (Figures 3C and 3E). Consistently, blockade of vn/Egfr signaling via knockdown of *Egfr* or its downstream *Ras85D*, but not blockade of Pvf1/Pvr signaling via overexpressing a dominant negative Pvr (*Pvr.DN*), terminated yki^{3SA}-tumor growth (Figure 3F). These results indicate that yki^{3SA}-tumor cells produce vn to activate autonomous Egfr/MEK signaling and promote growth.

yki^{3SA} Tumors Produce Pvf1 to Activate Host Pvr/MEK Signaling and Result in Host Wasting

We next confirmed Pvf1 expression in the ISCs (Figure 3G) and found that *Pvf1* knockdown in yki^{3SA} tumors suppressed pdERK levels significantly in the fat body and moderately in muscles and subsequently improved systemic wasting, including TAG decline, trehalose elevation, and muscle defects, in tumor-bearing flies (Figures 3H–3K). We also generated yki^{3SA}-tumors in *Pvf1*-null mutant flies (Wu et al., 2009) and confirmed that systemic removal of *Pvf1* also significantly alleviated the wasting effects in host tissues without perturbing yki^{3SA}-tumor growth (Figures 3M and 3N). Despite restoration of host wasting, *Pvf1* knockdown in yki^{3SA} tumors failed to extend longevity of tumor-bearing flies (Figure 3L), indicating that tumor-associated mortality involves other processes than host energy regulation. Since *vn* knockdown diminished tumor growth, systemic wasting effects were not observed in flies bearing yki^{3SA} tumors with *vn* RNAi (Figures 3K and 3L).

We further validated the autonomous effects of Pvr/MEK signaling by overexpressing an active form of Pvr (Pvr.λ) in the host tissues. Consistently, Pvr gain of function in the fat body resulted in MEK activation, lipid loss, and trehalose elevation (Figures 4A–4C), while in muscle, it potently caused climbing defects (Figures 4D and 4E). To mimic Pvf1 induction in yki^{3SA}-tumor-bearing midgut, we further overexpressed *Pvf1* in wild-type enterocytes and found MEK activation in both muscle and fat body and wasting effects, even though no obvious abdomen bloating was observed (Figures 4F and 4G). Note that Tram administration in flies bearing yki^{3SA}+dERK^{SEM} tumors failed to affect Pvf1 levels in the midgut (Figures S3J and S3K), suggesting that Tram suppresses host MEK signaling independent of midgut Pvf1. Collectively, our results demonstrate that yki^{3SA}-gut tumors produce Pvf1 to non-autonomously enhance Pvr/MEK signaling in host tissues and cause wasting.

Pvf1 and ImpL2 Are Independent Regulators of yki^{3SA}-Tumor-Associated Host Wasting

We previously showed that yki^{3SA}-tumor-derived ImpL2 contributes to host wasting (Kwon et al., 2015). Thus, we wondered whether ImpL2 and Pvf1 are independent regulators. We first examined whether tumor-derived ImpL2 affects host MEK signaling and found that *ImpL2* knockdown in yki^{3SA} tumors failed to suppress host pdERK (Figure 4I). In addition, MEK suppression does not impinge on tumor-derived ImpL2 to affect wasting, as administration of 10 μM Tram in flies bearing yki^{3SA}+dERK^{SEM} tumors failed to affect tumor ImpL2 production, brain ILPs levels, as well as feeding behavior (Figures S3K–S3M). Similarly, *Pvf1* removal in yki^{3SA}-gut tumors also barely affected tumor ImpL2 production (Figure S3N). To examine a potential

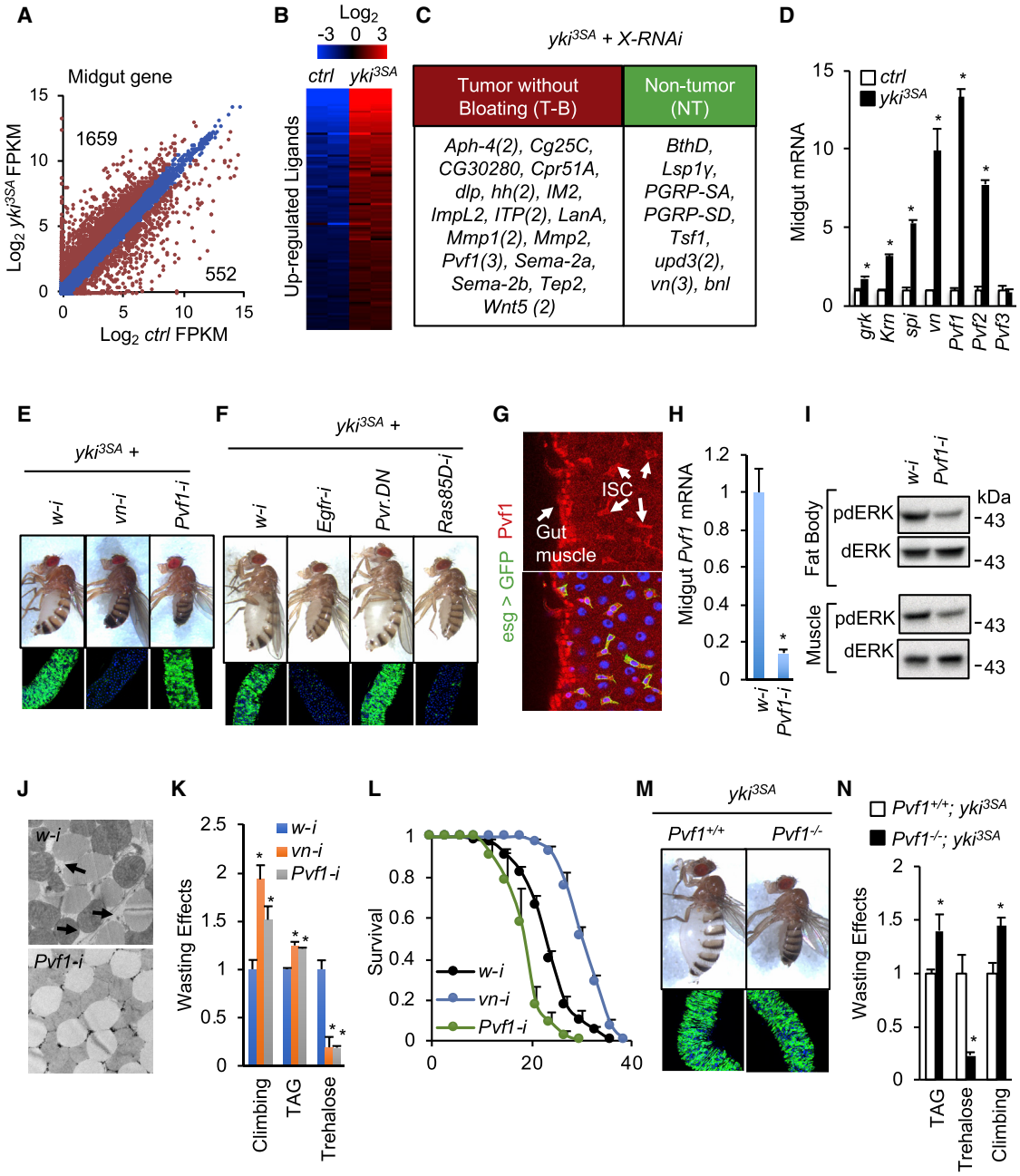

Figure 3. yki^{3SA}-Gut Tumors Cause Host MEK Activation and Wasting via Pvf1 Production

(A) Scatterplots comparing gene expression in *ctrl* and *yki^{3SA}* midguts.

(B) Heatmap showing up-regulated genes that encode secreted proteins.

(C) Bloating and tumor phenotypes of flies bearing gut-yki^{3SA} tumors with RNAi against ligand-encoding genes.

(D) RTK-ligand expressions in yki^{3SA}-tumor midguts at day 8 (n = 3, 30 midguts/group).

(E–L) Wasting phenotypes of flies bearing yki^{3SA}-tumor with indicated transgenes (*esg-GAL4, UAS-GFP, tub-GAL80^{TS}/+; UAS-yki^{3SA}/UAS-X*). Bloating (E and F) (up), gut tumors (E and F) (down), *Pvf1* expression (G) (antibody staining in control midgut) and (H) (n = 3, 30 midguts/group), pdERK (I), muscle degeneration (J), lipid and trehalose levels (K) (n = 3, 30 flies/group), climbing speeds (K) (n = 60), and lifespans (L) (n = 120).

(M and N) Bloating and gut phenotypes (M) and wasting effects, including TAG and trehalose levels (n = 3, 30 flies/group) and climbing speed (n = 60) (N), in *Pvf1*-null flies bearing *yki^{3SA}*-gut tumor (*Pvf1^{-}/Pvf1^{-}; esg-GAL4, UAS-GFP, tub-GAL80^{TS}/+; UAS-yki^{3SA}/+*).

Data are presented as means ± SEM. *p < 0.05.

crosstalk between Pvf1 and ImpL2, we knocked down both *Pvf1* and *ImpL2* in yki^{3SA} tumors. Surprisingly, as compared to knockdown of either *Pvf1* or ImpL2, double knockdown of these two ligands in yki^{3SA} tumors further alleviated host wasting, including bloating rates, lipid loss, as well as hyperglycemia, without affecting tumor growth (Figures 4J and 4K). Taken together,

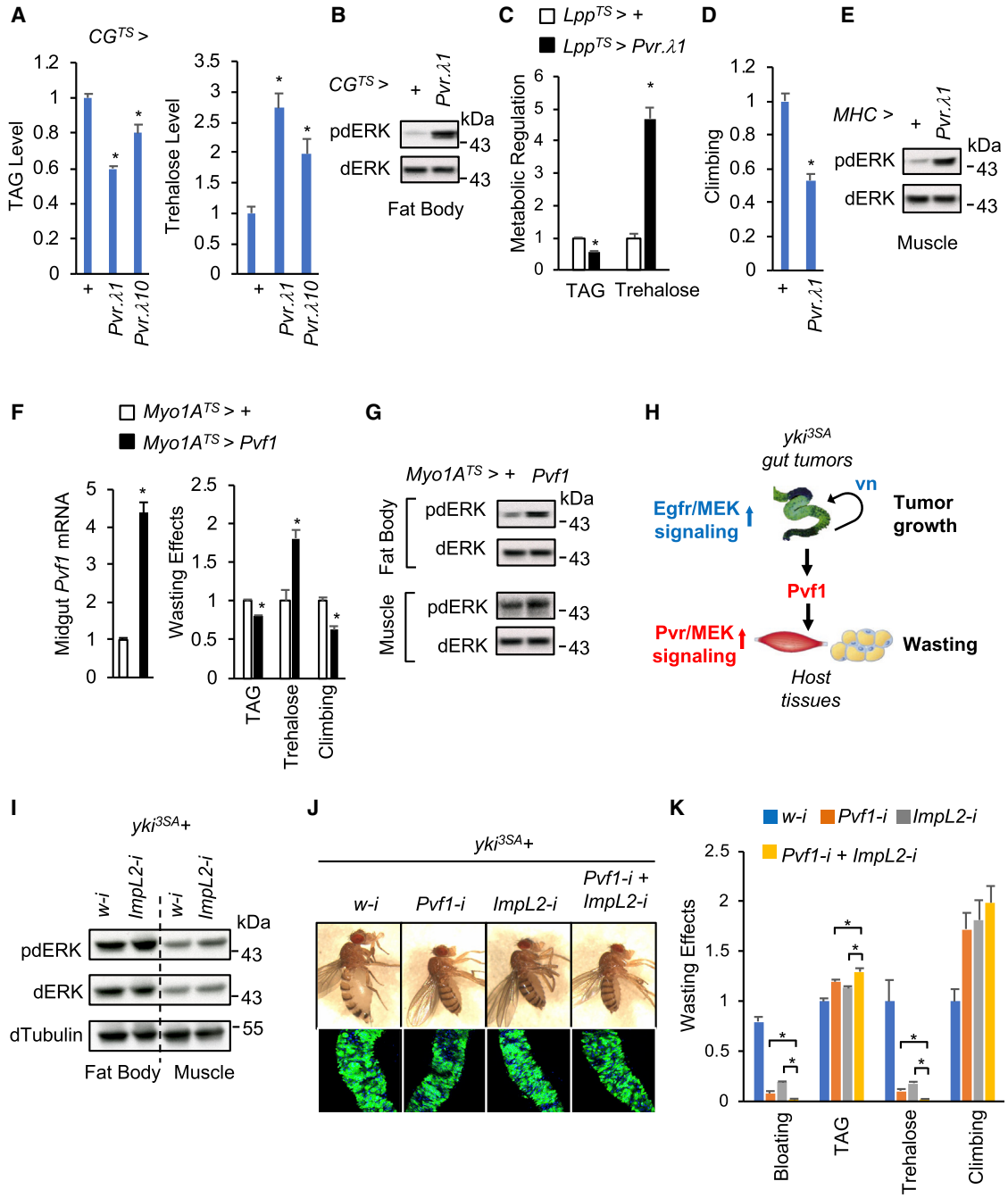

Figure 4. Pvf1/Pvr Axis Regulates MEK Activation and Host Wasting

(A–C) TAG and trehalose levels (A and C) (n = 3, 30 flies/group) and pdERK (B) in wild-type flies with fat body Pvr activation at 29°C for 4 days.

(D and E) Climbing speed (D) (n = 60) and pdERK (E) in wild-type flies with muscle Pvr activation at day 8.

(F and G) Midgut *Pvf1* mRNA (F) (left) (n = 3, 30 midguts/group), wasting effects (F) (right); including TAG and trehalose levels (n = 3, 30 flies/group) and climbing speed (n = 60), and pdERK (G) in flies with enterocyte *Pvf1* overexpression at 29°C for 8 days.

(H) Ligand-associated dual-MEK regulation of tumor growth and host wasting.

(I) pdERK in flies bearing yki^{3SA}-tumors with *ImpL2* RNAi (*esg-GAL4, UAS-GFP, tub-GAL80^{TS}/UAS-ImpL2-RNAi*-NIG15009R-3; *UAS-yki^{3SA}*/+).

(J and K) Bloating and gut tumors (J) and wasting effects (K); including bloating rates (n = 3, 60 flies/group), TAG and trehalose levels (n = 3, 30 flies/group), as well as climbing speeds (n = 60) of flies bearing yki^{3SA} tumors with RNAi at day 10. *UAS-Pvf1-RNAi*-NIG7103R-1 and *UAS-ImpL2-RNAi*-VDRC30931 were used.

Data are presented as means ± SEM. *p < 0.05.

our results demonstrate that yki^{3SA}-tumor-derived Pvf1 and ImpL2 are independent regulators of host wasting.

DISCUSSION

MEK/ERK Signaling Induces Muscle Wasting and Lipid Loss

Lipid loss and protein degradation-associated muscle wasting are two major features of tumor-induced host wasting in mammals (Fearon et al., 2013). We observe similar outcomes in yki^{3SA}-tumor-bearing flies and show that the MEK/ERK pathway acts as a critical pathogenic factor. Although the molecular mechanisms of MEK action in fly are unknown, our results are reminiscent of some mammalian studies. For example, MEK signaling was found to regulate ubiquitination-associated proteolysis in mouse myotubes and promote lipid mobilization in mammalian adipocytes (Hong et al., 2018; Zheng et al., 2010). We further confirmed similar MEK regulation in mammalian wasting models. Therefore, our study reveals that host MEK signaling plays a conserved role in tumor-induced wasting, including muscle wasting and lipid loss.

Ligand-Mediated Dual-MEK Regulation of Tumor-Host Interaction

The mechanism underlying the regulation of MEK signaling in tumor-induced host wasting is poorly understood. Here, we identified the secreted protein Pvf1 as a tumor-derived factor activating host MEK signaling. Pvr, the Pvf1 receptor, is expressed in both fat body and muscle (Kwon et al., 2015; Zheng et al., 2017). Activation of Pvf/Pvr signaling by overexpressing an active form of Pvr in the muscle and fat body is sufficient to cause muscle wasting and lipid loss, respectively. Reducing *Pvf1* production in yki^{3SA}-gut tumors decreased host MEK signaling and robustly alleviated wasting effects, while *Pvf1* overexpression in wild-type midgut enterocytes somehow mimicked tumor-induced wasting effects, confirming that yki^{3SA}-gut tumor-derived Pvf1 non-autonomously promotes host MEK signaling and wasting. Note that as compared to pharmaceutical MEK inhibition in host tissues, Pvf1 removal from yki^{3SA}-gut tumors fails to prolong survival suggesting that systemic regulation of survival is more complicated than energy wasting in the context of tumor growth. We speculate that Pvf1/Pvr/MEK signaling is missing from some host tissues and that additional MEK-activating ligands produced either directly from yki^{3SA} tumors or indirectly in host tissues contribute to mortality.

Autonomous MEK activation in yki^{3SA}-gut tumors is required for tumor growth. We demonstrate that only *vn*, a MEK-activating ligand essential for ISC proliferation (Xu et al., 2011), is critical for yki^{3SA}-gut tumor growth by activating Egfr/MEK signaling. Altogether, we propose a dual-MEK regulatory model whereby yki^{3SA}-gut tumors produce vn to autonomously promote self-growth, and Pvf1 to non-autonomously trigger Pvr/MEK signaling in host tissues and cause wasting (Figure 4H).

Organ Wasting Involves Energy Balance that Is Regulated by Multiple Tumor-Derived Ligands

We have previously shown that yki^{3SA}-gut tumors produce ImpL2 to suppress systemic insulin signaling and anabolism, which contribute to host wasting. However, ImpL2 removal from yki^{3SA}-gut tumors fails to completely abolish host wasting (Kwon et al., 2015), suggesting the existence of other cachectic factor(s). Here, we demonstrate that yki^{3SA}-gut tumors also produce Pvf1 that remotely promotes MEK signaling and catabolism in host tissues and causes wasting. Further, removal of both *ImpL2* and *Pvf1* in yki^{3SA}-gut tumors exhibits additive improvement of host wasting, as compared to removal of either *Impl2* or *Pvf1*. Thus, yki^{3SA}-gut tumors produce, at least, Pvf1 and ImpL2 to orchestrate organ wasting, involving both MEK and insulin signaling-associated catabolism and anabolism, respectively.

Interestingly, induction of these cachectic ligands is highly tumor-context dependent. Compared to yki^{3SA}, overexpression of a mild active form, yki^{S168A} (Oh and Irvine, 2009), in the ISCs only results in weak tumor growth, mild induction of *Pvf1* and *ImpL2*, and slight host wasting (data not shown). In *Ras^{V12}scrib^{-}* imaginal disc tumors (Figueroa-Clarevega and Bilder, 2015), only *ImpL2*, but not *Pvf1*, is highly induced (data not shown). Our study also suggests other potential cachectic factors in yki^{3SA} tumors, as removal of other ligands than ImpL2 and Pvf1 diminished bloating as well (Figure 3C). As tumor-induced wasting is a complicated physiological process, it is not surprising to observe differential involvement of multiple ligands/regulators. Further studies will be needed to characterize the functions of tumor-derived ligands and the intricate cross-talks between them.

Relevance to MEK Cascade and Cancer Cachexia

In addition to flies and mouse cells, we also observed that Tram remarkably abolished MEK activation in host tissues and improved wasting in LLC-tumor-bearing mice (data not shown). However, we cannot conclude the beneficial effects from host MEK inhibition, as Tram also reduced tumor sizes by 50% (data now shown). Thus, we speculate that the inconsistent results of MEK inhibition (Au et al., 2016; Quan-Jun et al., 2017) might be caused by different tumor responses to MEK inhibitors. To address the impact of MEK inhibition in host tissues but not in tumors, we generated drug-resistant yki^{3SA}+dERK^{SEM}-gut tumors in flies. Strikingly, MEK inhibitors, while no longer affecting tumor growth or tumor-derived ligand production, remarkably suppressed MEK signaling in host tissues (fat body, muscle, and maybe other secondary responsive organs) and abolished energy wasting. Thus, our results indicate that host MEK suppression is sufficient to reduce systemic wasting. Meanwhile, it will be worthy to obtain drug-resistant LLC cancer cells, via either random mutagenesis or genetic manipulation of MEK/ERK pathway, and evaluate the effects of MEK inhibitors in mice bearing drug-resistant LLC tumors in the future.

Finally, our results provide genetic evidence of tumor-secreted proteins, rather than systemic inflammatory responses, in tumor-induced wasting. VEGF exists in mammals as a homolog of *Drosophila* Pvf1 and activates Ras/MEK signaling (Holmes and Zachary, 2005). Similar to cachectic fly Pvf1, VEGF has been reported to be associated with lipid mobilization and muscle atrophy in mice (Gao et al., 2015; Sun et al., 2012). Administration of antibodies against VEGF or VEGFR-2 elicits beneficial effects on multiple organs and prolongs survival of mice bearing high-VEGF tumors (Xue et al., 2008). However, other tumor-derived ligands, including LIF and ILs, are also important MEK-activating factors and are associated with systemic catabolism (Miyamoto et al.,

2016; Seto et al., 2015). We therefore propose that cachectic tumors might produce multiple MEK-activating ligands to trigger organ wasting in mice and patients.

STAR★METHODS

Detailed methods are provided in the online version of this paper and include the following:

- KEY RESOURCES TABLE
- CONTACT FOR REAGENT AND RESOURCE SHARING
- EXPERIMENTAL MODEL AND SUBJECT DETAILS
  - Fly Strains
  - Cell Lines
- METHOD DETAILS
  - Gut Tumor Induction
  - Protein Degradation
  - Lipid and Carbohydrate Measurements in Flies
  - Lipolysis Measurements
  - Climbing Activity
  - Immunostainings
  - Western Blot
  - RNA-Seq Analysis of Adult Midgut
  - qPCR
  - Electron Microscopy
- QUANTIFICATION AND STATISTICAL ANALYSIS

SUPPLEMENTAL INFORMATION

Supplemental Information includes four figures and two tables and can be found with this article online at https://doi.org/10.1016/j.devcel.2018.12.003.

ACKNOWLEDGMENTS

We thank Arpan Ghosh, Ben Ewen-Campen, Pedro Saavedra, and Charles Xu for comments; Tian Xu and Xianjue Ma for *eyFLP1-FRT* and $Ras^{V12}scrib^{1}$ lines; Michael J. Galko for *Pvf1*-null mutant; Benny Shilo for Pvf1 antibody; and Hugo Stocker for ILP2 antibody. This work was supported in part by the American Diabetes Association (1-16-PDF-108). Work in the Perrimon lab is supported by NIH grants R01AR057352 and P01CA120964. N.P. is an Investigator of the Howard Hughes Medical Institute.

AUTHOR CONTRIBUTIONS

W.S. conceived the study and performed experiments. S.K. and B.S. performed tumor-bearing-mice experiments. S.H. and A.B. performed ERK inhibition and lipolysis in 3T3-L1 adipocytes. Y.H. and V.C. analyzed RNA-seq data. X.W. performed western blots. R.B. performed RNAi screening. H.-W.T. performed adult clonal analysis. W.S. and N.P. discussed results and wrote manuscript.

DECLARATION OF INTERESTS

The authors declare no competing interests.

Received: October 16, 2017
Revised: November 21, 2018
Accepted: December 4, 2018
Published: January 10, 2019

REFERENCES

Au, E.D., Desai, A.P., Koniaris, L.G., and Zimmers, T.A. (2016). The MEK-inhibitor selumetinib attenuates tumor growth and reduces IL-6 expression but does not protect against muscle wasting in Lewis lung cancer cachexia. Front. Physiol. *7*, 682.

Broughton, S., Alic, N., Slack, C., Bass, T., Ikeya, T., Vinti, G., Tommasi, A.M., Driege, Y., Hafen, E., and Partridge, L. (2008). Reduction of DILP2 in Drosophila triages a metabolic phenotype from lifespan revealing redundancy and compensation among DILPs. PLoS One *3*, e3721.

Chevalier, S., and Farsijani, S. (2014). Cancer cachexia and diabetes: similarities in metabolic alterations and possible treatment. Appl. Physiol. Nutr. Metab. *39*, 643–653.

Fearon, K., Arends, J., and Baracos, V. (2013). Understanding the mechanisms and treatment options in cancer cachexia. Nat. Rev. Clin. Oncol. *10*, 90–99.

Figueroa-Clarevega, A., and Bilder, D. (2015). Malignant Drosophila tumors interrupt insulin signaling to induce cachexia-like wasting. Dev. Cell *33*, 47–55.

Friedman, A., and Perrimon, N. (2006). High-throughput approaches to dissecting MAPK signaling pathways. Methods *40*, 262–271.

Gao, X., Zhao, Y., Stemmer-Rachamimov, A.O., Liu, H., Huang, P., Chin, S., Selig, M.K., Plotkin, S.R., Jain, R.K., and Xu, L. (2015). Anti-VEGF treatment improves neurological function and augments radiation response in NF2 schwannoma model. Proc. Natl. Acad. Sci. USA *112*, 14676–14681.

Holmes, D.I., and Zachary, I. (2005). The vascular endothelial growth factor (VEGF) family: angiogenic factors in health and disease. Genome Biol. *6*, 209.

Hong, S., Song, W., Zushin, P.H., Liu, B., Jedrychowski, M.P., Mina, A.I., Deng, Z., Cabarkapa, D., Hall, J.A., Palmer, C.J., et al. (2018). Phosphorylation of beta-3 adrenergic receptor at serine 247 by ERK MAP kinase drives lipolysis in obese adipocytes. Mol. Metab. *12*, 25–38.

Hu, Y., Comjean, A., Perkins, L.A., Perrimon, N., and Mohr, S.E. (2015). GLAD: an online database of gene list annotation for Drosophila. J. Genomics *3*, 75–81.

Kir, S., White, J.P., Kleiner, S., Kazak, L., Cohen, P., Baracos, V.E., and Spiegelman, B.M. (2014). Tumour-derived PTH-related protein triggers adipose tissue browning and cancer cachexia. Nature *513*, 100–104.

Kwon, Y., Song, W., Droujinine, I.A., Hu, Y., Asara, J.M., and Perrimon, N. (2015). Systemic organ wasting induced by localized expression of the secreted insulin/IGF antagonist ImpL2. Dev. Cell *33*, 36–46.

Liu, Q., Xu, W.G., Luo, Y., Han, F.F., Yao, X.H., Yang, T.Y., Zhang, Y., Pi, W.F., and Guo, X.J. (2011). Cigarette smoke-induced skeletal muscle atrophy is associated with up-regulation of USP-19 via p38 and ERK MAPKs. J. Cell. Biochem. *112*, 2307–2316.

Miyamoto, Y., Hanna, D.L., Zhang, W., Baba, H., and Lenz, H.J. (2016). Molecular pathways: cachexia signaling-a targeted approach to cancer treatment. Clin. Cancer Res. *22*, 3999–4004.

Oh, H., and Irvine, K.D. (2009). In vivo analysis of Yorkie phosphorylation sites. Oncogene *28*, 1916–1927.

Patel, P.H., and Edgar, B.A. (2014). Tissue design: how Drosophila tumors remodel their neighborhood. Semin. Cell Dev. Biol. *28*, 86–95.

Prado, C.M.M., Bekaii-Saab, T., Doyle, L.A., Shrestha, S., Ghosh, S., Baracos, V.E., and Sawyer, M.B. (2012). Skeletal muscle anabolism is a side effect of therapy with the MEK inhibitor: selumetinib in patients with cholangiocarcinoma. Br. J. Cancer *106*, 1583–1586.

Quan-Jun, Y., Yan, H., Yong-Long, H., Li-Li, W., Jie, L., Jin-Lu, H., Jin, L., Peng-Guo, C., Run, G., and Cheng, G. (2017). Selumetinib attenuates skeletal muscle wasting in murine cachexia model through ERK inhibition and AKT activation. Mol. Cancer Ther. *16*, 334–343.

Reiher, W., Shirras, C., Kahnt, J., Baumeister, S., Isaac, R.E., and Wegener, C. (2011). Peptidomics and peptide hormone processing in the Drosophila midgut. J. Proteome Res. *10*, 1881–1892.

Rohm, M., Schäfer, M., Laurent, V., Üstünel, B.E., Niopek, K., Algire, C., Hautzinger, O., Sijmonsma, T.P., Zota, A., Medrikova, D., et al. (2016). An AMP-activated protein kinase-stabilizing peptide ameliorates adipose tissue wasting in cancer cachexia in mice. Nat. Med. *22*, 1120–1130.

Rosin, D., Schejter, E., Volk, T., and Shilo, B.Z. (2004). Apical accumulation of the Drosophila PDGF/VEGF receptor ligands provides a mechanism for triggering localized actin polymerization. Development *131*, 1939–1948.

Seto, D.N., Kandarian, S.C., and Jackman, R.W. (2015). A key role for leukemia inhibitory factor in C26 cancer cachexia. J. Biol. Chem. *290*, 19976–19986.

Slack, C., Alic, N., Foley, A., Cabecinha, M., Hoddinott, M.P., and Partridge, L. (2015). The Ras-erk-ETS-signaling pathway is a drug target for longevity. Cell *162*, 72–83.

Song, W., Cheng, D., Hong, S., Sappe, B., Hu, Y., Wei, N., Zhu, C., O'Connor, M.B., Pissios, P., and Perrimon, N. (2017a). Midgut-derived activin regulates glucagon-like action in the fat body and glycemic control. Cell Metab. *25*, 386–399.

Song, W., Owusu-Ansah, E., Hu, Y., Cheng, D., Ni, X., Zirin, J., and Perrimon, N. (2017b). Activin signaling mediates muscle-to-adipose communication in a mitochondria dysfunction-associated obesity model. Proc. Natl. Acad. Sci. USA *114*, 8596–8601.

Song, W., Veenstra, J.A., and Perrimon, N. (2014). Control of lipid metabolism by tachykinin in Drosophila. Cell Rep. *9*, 40–47.

Sun, K., Wernstedt Asterholm, I., Kusminski, C.M., Bueno, A.C., Wang, Z.V., Pollard, J.W., Brekken, R.A., and Scherer, P.E. (2012). Dichotomous effects of VEGF-A on adipose tissue dysfunction. Proc. Natl. Acad. Sci. USA *109*, 5874–5879.

Takashima, S., Adams, K.L., Ortiz, P.A., Ying, C.T., Moridzadeh, R., Younossi-Hartenstein, A., and Hartenstein, V. (2011). Development of the Drosophila entero-endocrine lineage and its specification by the Notch signaling pathway. Dev. Biol. *353*, 161–172.

Wu, Y., Brock, A.R., Wang, Y., Fujitani, K., Ueda, R., and Galko, M.J. (2009). A blood-borne PDGF/VEGF-like ligand initiates wound-induced epidermal cell migration in Drosophila larvae. Curr. Biol. *19*, 1473–1477.

Xu, N., Wang, S.Q., Tan, D., Gao, Y., Lin, G., and Xi, R. (2011). EGFR, Wingless and JAK/STAT signaling cooperatively maintain Drosophila intestinal stem cells. Dev. Biol. *354*, 31–43.

Xue, Y., Religa, P., Cao, R., Hansen, A.J., Lucchini, F., Jones, B., Wu, Y., Zhu, Z., Pytowski, B., Liang, Y., et al. (2008). Anti-VEGF agents confer survival advantages to tumor-bearing mice by improving cancer-associated systemic syndrome. Proc. Natl. Acad. Sci. USA *105*, 18513–18518.

Zhang, G., Liu, Z., Ding, H., Miao, H., Garcia, J.M., and Li, Y.P. (2017). Toll-like receptor 4 mediates Lewis lung carcinoma-induced muscle wasting via coordinate activation of protein degradation pathways. Sci. Rep. *7*, 2273.

Zheng, B., Ohkawa, S., Li, H., Roberts-Wilson, T.K., and Price, S.R. (2010). FOXO3a mediates signaling crosstalk that coordinates ubiquitin and atrogin-1/MAFbx expression during glucocorticoid-induced skeletal muscle atrophy. FASEB J. *24*, 2660–2669.

Zheng, H., Wang, X., Guo, P., Ge, W., Yan, Q., Gao, W., Xi, Y., and Yang, X. (2017). Premature remodeling of fat body and fat mobilization triggered by platelet-derived growth factor/VEGF receptor in Drosophila. FASEB J. *31*, 1964–1975.

STAR★METHODS

KEY RESOURCES TABLE

REAGENT or RESOURCE	SOURCE	IDENTIFIER
Antibodies		
Rabbit anti-pERK	Cell Signaling Technology	Cat# 4370; RRID: AB_2315112
Rabbit anti-ERK	Cell Signaling Technology	Cat# 4695; RRID: AB_390779
Mouse anti-α-Tubulin	Sigma-Aldrich	Cat# T5168; RRID: AB_477579
Mouse anti-Prospero	Developmental Studies Hybridoma Bank	Cat# Prospero (MR1A); RRID: AB_528440
Mouse anti-MHC	Developmental Studies Hybridoma Bank	Cat# MF 20; RRID: AB_2147781
Rabbit anti-ILP2	Broughton et al., 2008	N/A
Rat anti-Pvf1	Rosin et al., 2004	N/A
Chemicals, Peptides, and Recombinant Proteins		
TRizol reagent	Thermo Fisher Scientific	15596018
iScript Reverse Transcription Supermix	Bio-Rad	1708896
iQ SYBR Green Supermix	Bio-Rad	1708880
Protease and phosphatase inhibitor cocktail	Pierce	78440
Glycerol standard	Sigma-Aldrich	G7793-5ML
D-(+)-Glucose	Sigma-Aldrich	G7021
Trehalase	Megazyme	K-TREH
PD0325901	Selleckchem	S1036
Trametinib	Selleckchem	S2673
DMEM, High glucose	Thermo Fisher Scientific	11965092
DMEM, High Glucose, HEPES, no Phenol Red	Thermo Fisher Scientific	21063029
Fetal Bovine Serum	Thermo Fisher Scientific	10437028
Horse Serum	Thermo Fisher Scientific	16050130
Bovine Serum Albumin	Sigma-Aldrich	A7030-1KG
IBMX	Sigma-Aldrich	I5879
Dexamethasone	Sigma-Aldrich	D1756
Rosiglitazone	Sigma-Aldrich	R2408
Insulin	Sigma-Aldrich	I2643
(Hydroxypropyl)methyl cellulose	Sigma-Aldrich	H7509
Paraformaldehyde 16% Solution	Fisher Scientific	50-980-487
[^{3}H]-tyrosine	PerkinElmer	NET127250UC
M3 Insect Medium	Sigma-Aldrich	S8398
Bodipy 493/503	Thermo Fisher Scientific	D3922
Critical Commercial Assays		
Free glycerol reagent	Sigma-Aldrich	F6428-40ML
Triglyceride reagent	Sigma-Aldrich	T2449-10ML
Bradford Reagent	Sigma-Aldrich	B6916-500ML
D-Glucose Assay Kit	Megazyme	K-GLUC
Deposited Data		
Data files for RNA sequencing	This paper	GSE113728
Experimental Models: Cell Lines		
Mouse: C2C12	ATCC	N/A
Mouse: 3T3-L1	ATCC	N/A
Mouse: LLC	Kir et al., 2014	N/A

(*Continued on next page*)

Continued

REAGENT or RESOURCE	SOURCE	IDENTIFIER
Experimental Models: Organisms/Strains		
Esg-Gal4, UAS-GFP, tub-Gal80^{ts}	Kwon et al., 2015	N/A
Cg-Gal4	Song et al., 2017a	N/A
R4-Gal4	Song et al., 2017a	N/A
Lpp-Gal4	Song et al., 2017a	N/A
dMef2-Gal4	Song et al., 2017b	N/A
Mhc-Gal4	Song et al., 2017b	N/A
Myo1A-Gal4	Song et al., 2014	N/A
UAS-yki^{3SA}	BDSC	28817
UAS-Raf ^{F179}	BDSC	2033
UAS-rl	BDSC	36270
UAS-rl^{SEM}	BDSC	59006
UAS-N^{intra}	BDSC	52008
UAS-Pvf1	BDSC	58426
UAS-Pvr.λ.mp1 (Pvr.λ1)	BDSC	58428
UAS-Pvr.λ.mp10 (Pvr.λ10)	BDSC	58496
UAS-Pvr.DN	BDSC	58430
Pvf1-null (Vegf17E^{1624ex3})	Wu et al., 2009	N/A
UAS-dERK (rl)–RNAi	TRiP	HMS00173
UAS-Egfr-RNAi	TRiP	JF01368
UAS-Ras85D-RNAi	TRiP	HMS01294
UAS-ImpL2-RNAi	NIG	15009R-3
UAS-ImpL2-RNAi	VDRC	30931
UAS-vn-RNAi	NIG	10491R-2
UAS-Pvf1-RNAi	VDRC	102699
UAS-Pvf1-RNAi	NIG	7103R-1
Other RNAi lines	This paper	See Table S2
Oligonucleotides		
Primers for *Drosophila grk* qPCR F: GTCGCCGTCACAGATTGTTG R: GATTGAGCAACTCAACCGCG	This paper	N/A
Primers for *Drosophila Krn* qPCR F: CCGCTTTAATCGGCGCTTAC R: ATCGGGAAGGTGACATTCGG	This paper	N/A
Primers for *Drosophila spi* qPCR F: TGCGGTGAAGATAGCCGATC R: TTCGCATCGCTGTCCCATAA	This paper	N/A
Primers for *Drosophila vn* qPCR F: GAACGCAGAGGTCACGAAGA R: GAGCGCACTATTAGCTCGGA	This paper	N/A
Primers for *Drosophila Pvf1* qPCR F: CTGTCCGTGTCCGCTGAG R: CTCGCCGGACACATCGTAG	This paper	N/A
Primers for *Drosophila Pvf2* qPCR F: GGTGGTCCACATCACGAGAG R: CGACTTTGTCGCTGCATCTG	This paper	N/A
Primers for *Drosophila Pvf3* qPCR F: TCGTGAAGAGCAGTAAGCATCG R: AGGTGCAACTCAGTATGGTGG	This paper	N/A
Primers for *Drosophila ImpL2* qPCR F: AAGAGCCGTGGACCTGGTA R: TTGGTGAACTTGAGCCAGTCG	This paper	N/A

(*Continued on next page*)

Continued

REAGENT or RESOURCE	SOURCE	IDENTIFIER
Primers for *Drosophila Ilp2* qPCR F: ATGAGCAAGCCTTTGTCCTTC R: ACCTCGTTGAGCTTTTCACTG	This paper	N/A
Primers for *Drosophila Ilp3* qPCR F: ATGGGCATCGAGATGAGGTG R: CGTTGAAGCCATACACACAGAG	This paper	N/A
Primers for *Drosophila Ilp5* qPCR F: CGCTCCGTGATCCCAGTTC R: AGGCAACCCTCAGCATGTC	This paper	N/A
Primers for *Drosophila RpL32* qPCR F: GCTAAGCTGTCGCACAAATG R: GTTCGATCCGTAACCGATGT	This paper	N/A
Primers for Mouse *MHC2B* qPCR F: AGTCCCAGGTCAACAAGCTG R: TTTCTCCTGTCACCTCTCAACA	This paper	N/A
Primers for Mouse *UbC* qPCR F: CCAGTGTTACCACCAAGAAGG R: ACACCCAAGAACAAGCACAA	This paper	N/A
Primers for Mouse *USP19* qPCR F: GTGGCCCTCTCTCCTGAAAC R: GGCAATGGGAGACAGCTCTT	This paper	N/A
Primers for Mouse *β-actin* qPCR F: CGGTTCCGATGCCCTGAGGCTCTT R: CGTCACACTTCATGATGGAATTGA	This paper	N/A
Software and Algorithms		
Photoshop	Adobe	N/A
ImageJ	NIH	N/A
Excel	Microsoft	N/A
MeV_4_7	MeV team	N/A
GLAD	Hu et al., 2015	N/A
Other		
SMZ18	Nikon	N/A
Axioskop	Zeiss	N/A
TCS SP2 AOBS Confocal	Leica	N/A
CFX96 Real-Time System	Bio-Rad	N/A
Multi-sample tissuelyser-24	Shanghai Jingxin Technology	N/A

CONTACT FOR REAGENT AND RESOURCE SHARING

Further information and requests for resources and reagents should be directed to and will be fulfilled by the Lead Contact, Wei Song (songw@whu.edu.cn).

EXPERIMENTAL MODEL AND SUBJECT DETAILS

Fly Strains

Driver lines for the midgut ISC (*esg-GAL4, tub-GAL80^{TS}, UAS-GFP*) (Kwon et al., 2015), fat body (*CG-GAL4, tub-GAL80^{TS}*), (*tub-GAL80^{TS}; R4-Gal4*), and (*tub-GAL80^{TS}; Lpp-Gal4*), muscle (*tub-GAL80^{TS}; dMef2-GAL4*) and (*Mhc-Gal4*) (Song et al., 2017b), and midgut enterocytes (*tub-GAL80^{TS}; Myo1A-GAL4, UAS-GFP*) (Song et al., 2014) have been described previously. *UAS-yki^{3SA}* (#28817), *UAS-Raf ^{F179}* (#2033), *UAS-rl* (referred to as "*UAS-dERK*", #36270), *UAS-rl^{SEM}* (referred to as "*UAS-dERK^{SEM}*", #59006), *UAS-N^{intra}* (#52008), *UAS-Pvf1* (#58426), *UAS-Pvr.λ* (#58428 and 58496), *UAS-Pvr.DN* (#58430) were obtained from the Bloomington Drosophila Stock Center. *Pvf1*-null mutant line (*Vegf17E^{1624ex3}*) was a kind gift from Michael J Galko. *eyFLP1; Act5C>y^{+}>GAL4, UAS-GFP; [FRT]82B*, *tub-GAL80* and *UAS-Ras^{V12}, [FRT]82B, scrib^{1}* lines used to generated Ras^{V12}scrib^{1} tumors were obtained from Tian Xu and Xianjue Ma.

Established RNAi lines were obtained from Bloomington Drosophila Stock Center, TRiP at Harvard Medical School, VDRC Stock Center, and the NIG-FLY stock center, including: *UAS-dERK (rl)–RNAi* (TRiP HMS00173), *UAS-ImpL2-RNAi* (NIG 15009R-3 and VDRC 30931) (Kwon et al., 2015), *UAS-Egfr-RNAi* (TRiP JF01368) and *UAS-Ras85D-RNAi* (TRiP HMS01294). Multiple RNAi lines against Pvf1 (VDRC 102699, NIG 7103R-1 and R-2) or vn (TRiP HMC04390, VDRC 109437, NIG 10491R-2) exhibited similar phenotypes, thus only UAS-Pvf1-RNAi-VDRC 102699 and NIG 7103R-1 and UAS-vn-RNAi-NIG 10491R-2 were shown in Figures 3 and 4. Negative controls, w^{1118} and *UAS-w-RNAi*, exhibited similar phenotypes and only *UAS-w-RNAi* is shown in the figures. Others RNAi lines used for *in vivo* RNAi screening are shown in Table S2.

Cell Lines

Mouse pre-adipocyte 3T3-L1 and mouse myoblasts C2C12 were purchased from American Type Culture Collection (ATCC). C2C12 myoblasts (< 15 passages) were cultured in growth medium (DMEM with 10% FBS and antibiotics) and differentiated into myotubes in differentiation medium, DMEM containing 2% horse serum (ThermoFisher, 16050130), for 5 days at 37°C in 5% CO_2. 3T3-L1 pre-adipocytes were cultured in growth medium. For differentiation, after 2 days at full confluency (day 0), 3T3-L1 pre-adipocytes were switched into DMEM containing 10% FBS, 0.5 mM IBMX, 0.25 μM dexamethasone, 1 μg/mL insulin, and 2 μM rosiglitazone (Sigma) for 2 days (day 2), and switched to DMEM with 10% FBS, 1 μg/mL insulin, and 2 μM rosiglitazone for another 2 days (day 4). Differentiated 3T3-L1 adipocytes were then maintained in growth medium for at least 4 days. LLC mouse tumor cells were cultured in growth medium. For LLC-conditioned medium preparation, after reaching 80% confluency, LLC cells were washed with PBS and cultured in growth medium (for adipocytes) or differentiation medium (for myotube) for the next 24 hr. Then conditioned media were centrifuged at 1,200 *g* for 10 min, filtered with a 0.2 μM syringe filtered, and stored at -80°C or used immediately after 3:1 dilution with fresh medium.

METHOD DETAILS

Gut Tumor Induction

Crosses were set up with *esg-GAL4, tub-GAL80^{TS}*, *UAS-GFP* and *UAS-yki^{3SA}* or *UAS-dERK^{SEM}; UAS-yki^{3SA}* at 18°C to inactivate GAL4. 4-day-old adult progenies were placed at 29°C to induce the transgenes. For the *in vivo* RNAi screening of ligands in *yki^{3SA}*-tumor guts, different RNAi lines were crossed to *esg-GAL4, tub-GAL80^{TS}, UAS-GFP/CyO; UAS-yki^{3SA}/TM6B* at 18°C. Virgin progenies were maintained at 18°C for at least 8 days and then switched to 29°C to induce transgenes. Lipid and sugar levels, climbing speed, muscle morphology, gut morphology, and bloating phenotypes were all measured after switching to 29°C for 8 days. For drug treatment, flies were transferred onto food containing inhibitors at day 0 (simultaneously with tumor induction) or day 4 (after tumor formation). MEK/ERK inhibitors PD0325901 (S1036) and Trametinib (S2673) were purchased from Selleckchem.

Protein Degradation

To measure protein degradation rates in adult fly muscles, 20 flies were cultured on normal food at 29°C to induce tumors for 4 days and then transferred onto normal food with 5 μCi [^{3}H]-tyrosine (PerkinElmer, NET127250UC) for 2 days to label fly proteins. 10 flies were washed with PBS and the thorax parts were dissected and lysed with 500 μL RIPA buffer at 4°C. After centrifugation at 12,000 rpm for 10 min at 4°C, 400 μL supernatant was used for measurement of labeled proteins using 5 mL Ultima Gold liquid scintillation cocktail (PerkinElmer) and scintillation counter. Radioactivity values were referred to as "basal" level. The other 10 flies were then transferred to normal food without [^{3}H]-tyrosine for another 2 days. Similarly, radioactivity in the thoraces was measured and referred to as "wasted" level. The protein degradation rate was defined by subtracting "wasted" level from "basal" level and then normalized to protein levels. To measure protein degradation in mouse myotubes, 3d-differentiated C2C12 myotube were incubated with differentiation medium (2% horse serum) containing 1 μCi/mL [^{3}H]-tyrosine for 48h to label cellular proteins. The cells were washed with PBS and transferred to differentiation medium with 2 mM tyrosine for 2 hr to exclude short-lived proteins. Cells were then cultured with control or LLC-conditioned differentiation medium (3:1 diluted with normal differentiation medium) containing 2 mM tyrosine for 12 hr to measure release of [^{3}H]-tyrosine. 500 μL culture medium was mixed with 100 μL 10 mg/mL BSA and precipitated with 600 μL 20% (wt/vol) TCA overnight at 4°C. After centrifugation at 12,000 rpm for 5 min, the TCA-soluble radioactivity from supernatant, which reflect the protein degradation rate, was measured using scintillation counter.

Lipid and Carbohydrate Measurements in Flies

We measured fly TAG and carbohydrates as described previously (Kwon et al., 2015; Song et al., 2014). Briefly, 10 flies from each group were homogenized using Multi-sample Tissuelyser-24 (Shanghai Jingxin Technology) with 1 mL PBS containing 0.2% Triton X-100 and heated at 70°C for 5 min. The supernatant was collected after centrifugation at 14,000 rpm for 10 min at 4°C. 10 μl of supernatant was used for protein quantification using Bradford Reagent (Sigma, B6916-500ML). Whole body trehalose levels were measured from 10 μl of supernatant treated with 0.2 μl trehalase (Megazyme, E-TREH) at 37°C for 30 min using glucose assay reagent (Megazyme, K-GLUC) following the manufacturer's protocol. We subtracted the amount of free glucose from the measurement and then normalized the subtracted values to protein levels in the supernatant. To measure whole body triglycerides, we processed 10 μl of supernatant using a Serum Triglyceride Determination kit (Sigma, TR0100). We subtracted the amount of free glycerol from the measurement and then normalized the subtracted values to protein levels. To measure circulating trehalose concentrations, hemolymph was extracted from 20 decapitated adults by centrifugation at 1,500 g for 10 min. 0.5 μL collected hemolymph was diluted in

40 μl of PBS, heated at 70°C for 5 min, and centrifuged at 14,000 rpm at 4°C for 10 min. 10 μL supernatant was treated with 0.2 μl trehalase (Megazyme, E-TREH) at 37°C for 30 min and then used to measure circulating trehalose levels with glucose assay reagent (Megazyme, K-GLUC). We subtracted the amount of free glucose in the supernatant from the measurement.

Lipolysis Measurements

For lipolysis measurement in flies, 10 adult abdomens containing fat bodies with midguts removed were dissected and washed with 1 mL M3 Insect Medium (Sigma, S8398) at room temperature. Supernatant was aspirated after a brief centrifugation and 10 abdomens were incubated with 100 μL M3 medium containing 4% fatty-acid-free BSA (w/v, Sigma, A7030-1KG) with or without 1 μM Trametinib for 1 hr at room temperature. Released glycerol in M3 medium was determined using Free Glycerol Reagent (Sigma, F6428-40ML). Abdomens were later lysed in RIPA buffer and used for protein quantification with Bradford Reagent (Sigma, B6916-500ML). Final lipolysis rate was calculated by normalizing released glycerol level to abdomen protein amount. For lipolysis measurement in adipocytes, after treated with control or conditioned medium 24 hr, 3T3-L1 adipocytes were washed with PBS and incubated with serum- and phenol-free DMEM containing 4% fatty-acid-free BSA with or without trametinib for 1 hr. The glycerol amount in the medium was immediately measured using a Free Glycerol Reagent kit (F6428, Sigma). After treated with conditioned medium and drugs for 24h, 3T3-L1 adipocytes were washed and harvested in TNET buffer (50 mM Tris-HCl (pH7.4), 150 mM NaCl, 2 mM EDTA, and 1% Triton X-100) with 0.5% cholate. Dissolved TAG was measured using a Serum Triglyceride Determination kit (TR0100, Sigma) and normalized to protein level.

Climbing Activity

Ten flies were placed in an empty vial and then tapped down to the bottom. They were allowed to climb for 3 s. Climbing was recorded and climbing height and speed were calculated from the video. A minimum of 60 flies and 10 separate trials were run per condition.

Immunostainings

Brains, midguts, and abdomens containing fat bodies were dissected in PBS and fixed for 15 min in PBS containing 4% paraformaldehyde. After fixation, the samples were washed with PBS containing 0.2% Triton X-100 (PBST) and blocked with 1% BSA in PBST for 30 min. After incubation with primary antibodies overnight at 4°C: p-ERK (1:100, Cell Signaling, 4370), Prospero (1:100, DSHB, MR1A), ILP2 (1:1000, a kind gift from Hugo Stocker), or Pvf1 (1:50, a kind gift from Ben-Zion Shilo). Tissues were washed and then incubated with secondary antibody and DAPI for 1 hr, washed, and mounted in Vectashield (Vector). C2C12 myoblasts were cultured and differentiated on cover slides. Treated C2C12 myotubes were washed and fixed for 15 min in PBS containing 4% formaldehyde. After fixation, the samples were washed with PBST, blocked with 1% BSA in PBST, and incubated with primary antibody against MHC (1:50, DSHB, MF20) overnight at 4°C. Cells were then incubated with secondary antibody and DAPI for 1h, washed and mounted in Vectashield (Vector). Treated 3T3-L1 mature adipocytes were incubated with Bodipy 493/503 (1 μg/mL, Life Technologies, D3922) for 20 min, washed, and imaged. Regular microscopy was performed on a Zeiss Axioskop 2motplus or a Nikon SMZ18 and confocal images were obtained using a Leica system.

Western Blot

10 adult thoraces, 10 adult abdomens without midgut, and treated C2C12 myotubes and 3T3-L1 mature adipocytes were lysed in RIPA buffer containing inhibitors of proteases and phophatases. Extracts were immunoblotted with indicated antibodies: rabbit anti-ERK (1:1000, Cell Signaling, 4695), rabbit anti-phospho-ERK (1:1000, Cell Signaling, 4370), α-tubulin (1:5000, Sigma, T5168).

RNA-Seq Analysis of Adult Midgut

15 midguts of *ctrl* or *yki*^{3SA} flies incubated for 8 days at 29°C were dissected for total RNA extraction. After assessing RNA quality with Agilent Bioanalyzer (RIN > 7), total RNAs were sent to Columbia Genome Center for RNA-seq analysis following the standard protocol. Briefly, mRNAs were enriched by poly-A pull-down. Sequencing libraries were prepared with Illumina Truseq RNA preparation kit and were sequenced using Illumina HiSeq 2000. Samples were multiplexed in each lane, which yields target number of single-end 100-bp reads for each sample, as a fraction of 180 million reads for the whole lane. The RNA-seq data were deposited in the Gene Expression Omnibus (accession number GSE113728). After trimming, sequence reads were mapped to the *Drosophila* genome (FlyBase genome annotation version r6.15) using Tophat. With the uniquely mapped reads, gene expression was quantified using Cufflinks (FPKM values) and HTseq (read counts per gene). Differentially expressed genes were analyzed based on both adjusted *P* value using DSeq2 as well as fold change cut-off. Prior to fold change calculation, we set to a value of "1" for any FPKM value between 0 and 1 to reduce the possibility that we get large ratio values for genes with negligible levels of detected transcript in both experimental and control samples (e.g. FPKM 0.1 vs. 0.0001), as those ratios are unlikely to have biological relevance. A cut-off of 2-fold change consistently observed among replicates and the adjusted *P* value of 0.05 or lower from DSeq2 analysis were used as criteria to define the set of 552 down-regulated and 1659 up-regulated genes. Heatmap was generated using MEV_4_7 based on FPKM changes.

qPCR

10 adult midguts or heads of each genotype and C2C12 myotubes were lysed with Trizol for RNA extraction and cDNA transcribed using the iScript cDNA Synthesis Kit (Bio-rad). qPCR was then performed using iQ SYBR Green Supermix on a CFX96 Real-Time

System/C1000 Thermal Cycler (Bio-rad). *Drosophila* and mouse gene expression were normalized to *RpL32* and *β-actin*, respectively. qPCR primers are listed in STAR Methods.

Electron Microscopy

Adult thoraces were processed and analyzed in cross-section following standard protocols at Electron Microscopy Facility in Harvard Medical School. Briefly, thoraces were fixed in 0.1 M sodium cacodylate buffer (pH 7.4) containing 2.5% glutaraldehyde, 2% paraformaldehyde overnight. The fixed samples were washed in 0.1M cacodylate buffer, fixed again with 1% osmiumtetroxide (OsO4) and 1.5% potassium ferrocyanide (KFeCN6) for 1 hr, and washed 3 times in water. Samples were incubated in 1% aqueous uranyl acetate for 1 hr and followed by 2 washes in water and subsequent dehydration in grades of alcohol. The samples were then put in propyleneoxide for 1 hr and embedded in TAAB Epon (Marivac Canada Inc.). Ultrathin sections (about 60nm) were cut on a Reichert Ultracut-S microtome, moved to copper grids, and then stained with lead citrate. Sections were examined in a JEOL 1200EX Transmission electron microscope, and images recorded with an AMT 2k CCD camera.

QUANTIFICATION AND STATISTICAL ANALYSIS

Data are presented as the mean ± SEM. Unpaired Student's t test and one-way ANOVA followed by post-hoc test were performed to assess the differences. $p < 0.05$ was considered statistically significant.